Structure and Lithium Dynamics of Li_2AuSn_2—A Ternary Stannide with Condensed $AuSn_{4/2}$ Tetrahedra

Zhiyun Wu,[a] Bernd D. Mosel,[a] Hellmut Eckert,*[a] Rolf-Dieter Hoffmann,[b] and Rainer Pöttgen*[b]

Abstract: The new stannide Li_2AuSn_2 was prepared by reaction of the elements in a sealed tantalum tube in a resistance furnace at 970 K followed by annealing at 720 K for five days. Li_2AuSn_2 was investigated by X-ray diffraction on powders and single crystals and the structure was refined from single-crystal data: $Z=4$, $I4_1/amd$, $a=455.60(7)$, $c=1957.4(4)$ pm, wR2 = 0.0681, 278 F^2 values, 10 parameters. The gold atoms display a slightly distorted tetrahedral tin coordination with Au–Sn distances of 273 pm. These tetrahedra are condensed through common corners leading to the formation of two-dimensional $AuSn_{4/2}$ layers. The latter are connected in the third dimension through Sn–Sn bonds (296 pm). The lithium atoms fill distorted hexagonal channels formed by the three-dimensional $[AuSn_2]$ network. Modestly small ^{7}Li Knight shifts are measured by solid-state NMR spectroscopy that are consistent with a nearly complete state of lithium ionization. The noncubic local symmetry at the tin site is reflected by a nuclear electric quadrupolar splitting in the ^{119}Sn Mössbauer spectra and a small chemical shift anisotropy evident from ^{119}Sn solid-state NMR spectroscopy. Variable-temperature static ^{7}Li solid-state NMR spectra reveal motional narrowing effects at temperatures above 200 K, revealing lithium atomic mobility on the kHz time scale. Detailed lineshape as well as temperature-dependent spin lattice relaxation time measurements indicate an activation energy of lithium motion of 27 kJ mol^{-1}.

Keywords: alloy electrode · lithium · NMR spectroscopy · solid-state structures · stannides

Introduction

Intermetallic lithium alloys have become an attractive alternative to lithium metal or lithium–carbon intercalates as anode materials in nonaqueous electrochemical cells. Their features include relatively high lithium packing densities, high stabilities and hence, long life cycles.[1–4] In this context the stannide Li_2AuSn,[5] the intermetallic lithium compounds LiT_2X (T = transition metal and X = Group 14 element) with Heusler-type structure ($MnCu_2Al$ type)[6] and a variety of other intermetallics crystallizing in the CaF_2, ZnS, or LiAlSi structure types are promising candidate materials, and their implementation in nonaqueous batteries with charge capacities between 380 and 1400 mAh g^{-1} has been reported.[7]

Based on the promise of binary Li–Sn- and Li–Sb-based alloys for such applications, new materials in the ternary systems lithium/transition metal/tin have been investigated recently with respect to the crystal structures and lithium dynamics.[8] While no Li motion could be observed on the NMR time scale in LiAuSn[11,12] and in a series of compounds having the $LiTSn_4$ composition (T = Ru, Rh, Ir),[9,10] a reasonable degree of lithium mobility at accessible temperatures was detected recently in the cubic stannide $LiAg_2Sn$.[13] Here, temperature-dependent ^{7}Li NMR line shapes indicate motional narrowing above 473 K and an activation energy of 33 kJ mol^{-1} for the lithium diffusion.

During our systematic investigations of the lithium/gold/tin system we discovered the new lithium ion conductor Li_2AuSn_2.[14] In the present contribution we report the detailed structural characterization of this stannide and give evidence of fast lithium ion motion on the kHz time scale at temperatures near ambient.

Experimental Section

Synthesis: Starting materials for the preparation of Li_2AuSn_2 were lithium rods (Merck, >99%), gold wire (Degussa-Hüls, ∅1 mm, >99.9%),

[a] Dr. Z. Wu, Dr. B. D. Mosel, Prof. Dr. H. Eckert
Institut für Physikalische Chemie und Sonderforschungsbereich 458, Universität Münster
Schlossplatz 4/7, 48149 Münster (Germany)
E-mail: eckerth@uni-muenster.de

[b] Dr. R.-D. Hoffmann, Prof. Dr. R. Pöttgen
Institut für Anorganische und Analytische Chemie und Sonderforschungsbereich 458, Universität Münster
Wilhelm-Klemm-Strasse 8, 48149 Münster (Germany)
E-mail: pottgen@uni-muenster.de

DOI: 10.1002/chem.200305479

and a tin bar (Heraeus, >99.9 %). The lithium rods were cut into smaller pieces under dry paraffin oil and subsequently washed with *n*-hexane. The paraffin oil and *n*-hexane were dried over sodium wire. The lithium pieces were kept in Schlenk tubes under argon prior to the reactions. Argon was purified over a titanium sponge (900 K), silica gel, and molecular sieves. The lithium pieces were mixed with the gold wire and pieces of the tin bar in the ideal 2:1:2 atomic ratio under flowing argon, and then sealed in a tantalum ampoule under an argon pressure of about 800 mbar in an arc-melting apparatus.[15] The tantalum tube was subsequently enclosed in an evacuated silica tube for oxidation protection, rapidly heated to 970 K and held at this temperature for 14 h. The temperature was then lowered to 720 K over three hours and kept at this temperature for five days. Finally the tube was slowly cooled to room temperature within the furnace by switching off the power. The sample could be readily separated from the tube. No reaction with the container material was observed. The sample is kept in argon-filled Schlenk tubes because it is slightly sensitive to moist air. The polycrystals and single crystals exhibit metallic luster, while powders are dark gray.

Elemental analysis: Polycrystalline pieces of the sample have been analyzed with a LEICA 420 I scanning electron microscope. The EDX analyses were carried out with elemental gold and InAs as standards. The gold/tin ratio was close to 1:2. No metallic impurities were detected. Another part of the polycrystalline sample was analyzed by inductively coupled plasma optic emission spectrometry using a SPECTRO CIROS ICP-OES to get a reliable value for the lithium content. The sample was completely dissolved in aqua regia. Analyses revealed the composition $Li_{1.94(2)}AuSn_2$. No tantalum contaminants were observed.

X-ray diffraction: The purity of the sample was checked by a Guinier powder pattern using $Cu_{K\alpha1}$ radiation and α-quartz ($a=491.30$, $c=540.46$ pm) as an internal standard. The Guinier camera was equipped with an imaging plate detector (Fujifilm, Basread-1800). To ensure correct indexing, the observed pattern was compared with a calculated one[16] based on the positions of the refined structure. The refined lattice parameters are listed in Table 1.

Small single crystals of Li_2AuSn_2 were isolated from the bulk sample by mechanical fragmentation and examined on a Buerger precession camera equipped with an image plate system (Fujifilm Basread-1800) to get data both on the symmetry and on the suitability for collecting intensity data. Single-crystal intensity data were collected at room temperature by use of a four-circle diffractometer (CAD4) with graphite-monochromatized $Mo_{K\alpha}$ radiation (71.073 pm) and a scintillation counter with pulse height discrimination. The scans were performed in the $\omega/2\theta$ mode. An empirical absorption correction was applied on the basis of Ψ-scan data. All relevant crystallographic data and details of the data collection and evaluation are listed in Table 1.

Table 1. Crystal data and structure refinement for Li_2AuSn_2.

empirical formula	Li_2AuSn_2
formula weight [g mol^{-1}]	448.23
unit cell dimensions	
a [pm]	455.60(7)
c [pm]	1957.4(4)
V [nm^3]	0.4063
Pearson symbol	tI20
space group	$I4_1/amd$
Z	4
ρ_{calcd} [g cm^{-3}]	7.33
crystal size [μm^3]	15 × 20 × 20
transmission ratio (max min^{-1})	7.64
absorption coefficient [mm^{-1}]	48.0
F (000)	740
θ range for data collection	4° to 35°
range in hkl	±7, +6, $-31 \le l \le 1$
total no. of reflections	945
independent reflections	278 ($R_{int}=0.1190$)
reflections with $I > 2\sigma(I)$	183 ($R_{sigma}=0.0794$)
data/parameters	278/10
goodness-of-fit on F^2	0.954
final R indices [$I > 2\sigma(I)$]	$R1=0.0313$; $wR2=0.0613$
R indices (all data)	$R1=0.0593$; $wR2=0.0681$
extinction coefficient	0.0013(2)
largest diff. peak and hole	4.55 and −2.03 e Å^{-3}

Solid-state spectroscopy: A $Ca^{119m}SnO_3$ source was available for the ^{119}Sn Mössbauer spectroscopic investigation. The sample was placed within a thin-walled PVC container with a thickness of about 10 mg Sn cm^{-2}. A palladium foil with a thickness of 0.05 mm was used to reduce the tin K X-rays concurrently emitted by this source. The measurement was conducted in the usual transmission geometry at 78 K. Solid-state ^{119}Sn NMR spectra were recorded at 149.8 MHz, using a Bruker DSX 400 spectrometer equipped with a 4 mm MAS-NMR probe. Spectra were taken on samples spinning at a rate of 9 kHz with 90° pulses of 2 μs length, followed by relaxation delays of 0.5 s. Chemical shifts are reported relative to a tetraoctyltin standard ($\delta=-6.9$ ppm versus tetramethyltin). ^{7}Li NMR spectra were measured on a Bruker DSX 400 spectrometer, interfaced to 9.4 T and 4.7 T magnets. Data was acquired by using pulse lengths of 1.5 μs and relaxation delays between 10 and 15 s. Room-temperature magic angle spinning spectra (8 kHz) and static spectra in the temperature range 180 K $< T <$ 485 K were measured in a commercial 4 mm MAS-NMR probe. Additional experiments were carried out using a home-built probe operating at 77.7 MHz. Static lineshapes and ^{7}Li spin-lattice relaxation times (measured by the saturation recovery technique) were obtained on samples sealed in silica glass containers in the temperature range 320 K $< T <$ 810 K. Chemical shifts are reported with respect to a 1 M LiCl aqueous solution.

Abstract in German: *Das neue Stannid Li_2AuSn_2 wurde durch eine Reaktion der Elemente in einer geschlossenen Tantalampulle in einem Widerstandsofen bei 970 K synthetisiert und anschließend bei 720 K für fünf Tage getempert. Li_2AuSn_2 wurde anhand von Röntgen-Pulver- und Einkristalldaten charakterisiert und die Struktur wurde anhand von Einkristall-Diffraktometerdaten verfeinert: $Z=4$; $I4_1/amd$; $a=455.60(7)$; $c=1957.4(4)$ pm; $wR2=0.0681$; 278 F^2-Werte; 10 variable Parameter. Die Goldatome haben eine verzerrt tetraedrische Zinnkoordination mit Au-Sn Abständen von 273 pm. Diese Tetraeder sind über gemeinsame Ecken zu zweidimensionalen $AuSn_{4/2}$ Schichten verknüpft. In der dritten Dimension erfolgt die Verknüpfung der Schichten über Sn–Sn Bindungen (296 pm Sn–Sn Abstand). Die Lithiumatome füllen leicht verzerrte, hexagonale Kanäle innerhalb des dreidimensionalen $[AuSn_2]$ Netzwerkes. Die sehr geringe ^{7}Li Knight Verschiebung aus der Festkörper NMR-Messung weist auf eine fast vollständige Ionisierung des Lithiums hin. Die nicht-kugelsymmetrische lokale Symmetrie der Zinnatome manifestiert sich durch eine Quadrupolaufspaltung im ^{119}Sn Mössbauer Spektrum und durch eine kleine Anisotropie in der chemischen Verschiebung im ^{119}Sn Festkörper NMR Spektrum. Temperaturabhängige ^{7}Li Festkörper NMR Spektren zeigen eine Linienverschmälerung oberhalb von 200 K, was auf eine Lithiumbeweglichkeit auf der kHz Zeitskala hindeutet. Detaillierte Analysen der Linienbreiten und Spin-Gitter-Relaxationszeitmessungen zeigen eine Aktivierungsenergie von 27 kJ mol^{-1} für die Lithiumbeweglichkeit.*

Results and Discussion

Structure refinement: Analysis of the diffraction data revealed the centrosymmetric space group $I4_1/amd$. The atomic positions of the gold and tin atoms were determined from an interpretation of direct methods with SHELXS-97.[17] The lithium site was obtained from a difference Fourier synthesis. The structure was refined with SHELXL-97[18] with anisotropic displacement parameters for the gold and the tin sites, while lithium was refined isotropically. The occupancy parameters of gold and tin were refined in a separate series of least-squares cycles. Both sites are fully occupied within two standard deviations. In the final cycles, the ideal occupancies were assumed again. Besides the strongly scattering gold and tin atoms, it was not possible to refine reliably the occupancy parameter of lithium from the X-ray data. We have thus assumed the ideal composition Li_2AuSn_2 (see ICP analyses). The refinement results are listed in Table 1, 2, and 3. Further details may be obtained from the Fachinformationszentrum Karlsruhe, 76344 Eggenstein-Leopoldshafen, Germany (fax: (+49)7247-808-666;), e-mail: crysdata@fiz-karlsruhe.de) on quoting the depository number CSD-391242.

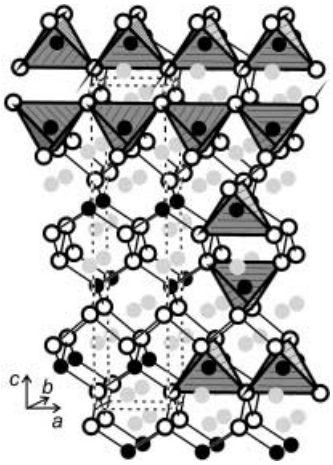

Figure 1. Crystal structure of tetragonal Li_2AuSn_2, space group $I4_1/amd$. Lithium, gold, and tin atoms are drawn as gray, filled, and open circles, respectively. The three-dimensional $[AuSn_2]$ polyanion and the condensed $AuSn_{4/2}$ tetrahedra are highlighted.

Table 2. Atomic coordinates and anisotropic displacement parameters [pm^2] for Li_2AuSn_2.

Atom	Wyckoff position	x	y	z	U_{11}	U_{22}	U_{33}	U_{eq}/U_{iso}[a]
Li	8*e*	0	1/4	0.551(1)	–	–	–	238(90)
Au	4*b*	1/2	1/4	1/8	89(3)	U_{11}	96(5)	91(3)
Sn	8*e*	0	1/4	0.04836(5)	83(4)	137(5)	33(7)	84(3)

[a] U_{eq} is defined as one third of the trace of the orthogonalized U_{ij} tensor. $U_{12}=U_{13}=U_{23}=0$

Table 3. Interatomic distances [pm] calculated with the powder lattice parameters in the structure of Li_2AuSn_2.

Li:	2	Au	270(1)	Au:	4	Li	270(1)
	1	Sn	295(3)		4	Sn	272.76(6)
	2	Sn	299(2)		2	Li	344(3)
	2	Li	302(4)	Sn	2	Au	272.76(6)
	4	Sn	322.19(6)		1	Li	295(3)
	1	Au	344(3)		2	Sn	296.2(1)
					2	Li	299(2)
					4	Li	322.19(6)

Crystal chemistry and chemical bonding: Li_2AuSn_2 crystallizes with a new structure type for intermetallic compounds. In Figure 1 we present a view of the unit cell. As emphasized in the left-hand part of Figure 1, the gold and tin atoms form a three-dimensional $[AuSn_2]$ polyanion in which the lithium atoms fill distorted hexagonal channels. Within the polyanion, each gold atom has four nearest tin neighbors in a slightly distorted tetrahedral coordination at Au–Sn distances of 273 pm, close to the sum of the covalent radii (274 pm).[19] In binary $AuSn_2$,[20] each gold atom has a distorted octahedral tin coordination at Au–Sn distances ranging from 272 to 284 pm. The $AuSn_4$ tetrahedra are condensed through common corners within the *ab* planes, leading to a two-dimensional network (Figure 1). These layers of $AuSn_{4/2}$ tetrahedra are connected by Sn–Sn bonds in the third dimension. All tin atoms are within zigzag chains, and the Sn–Sn distance of 296 pm lies between the corresponding values for α-Sn (4×281 pm) and β-Sn (4×302 pm; 2×318 pm).[21] Besides strong covalent Au–Sn bonding, we can assume also strong Sn–Sn bonding within the network.

The three coordination polyhedra for the Li_2AuSn_2 structure are presented in Figure 2. The lithium atoms have two lithium, three gold, and seven tin neighbors. The shortest distances occur for the Li–Au contacts (270 pm), close to the Li–Au distance in LiAu which has a CsCl-type structure[22] (268 pm), but somewhat longer than the sum of the covalent radii (257 pm).[19] Even longer Li–Au distances have been observed in the sulfides

Figure 2. Coordination polyhedra in the structure of Li_2AuSn_2. Lithium, gold, and tin atoms are drawn as grey, filled, and open circles, respectively. The site symmetries are indicated.

LiAuS (301 pm) and Li_3AuS_2 (308 and 328 pm).[23,24] The Li–Sn distances range from 295 to 322 pm, similar to those observed in $LiRuSn_4$[9] and in the complicated structures of the binary lithium stannides such as $Li_{4.4}Sn$.[25] Each lithium atom has two lithium neighbors at a distance of 302 pm, which is similar to *bcc* lithium (304 pm).[21] In saltlike Li_3AuS_2 an even shorter Li–Li distance of 292 pm occurs.[24] According to the ICP-OES analysis, the lithium position is not fully occupied. This leaves the vacancies that are most likely used for lithium diffusion.

Only the gold atoms lie on a special position and consequently they have the highest site symmetry ($\bar{4}m2$) in the Li_2AuSn_2 structure. The coordination polyhedron looks like a slightly distorted cube (Figure 2) and might be considered as two interpenetrating tetrahedra of lithium and tin atoms. The two lithium atoms capping the cube faces have longer Au–Li distances of 344 pm. The tin atoms have the same site symmetry as lithium (2 *mm.*) and a similar coordination polyhedron (Figure 2).

Figure 3 shows the ^{119}Sn MAS NMR spectrum of Li_2AuSn_2. The Knight shift of $\delta = 4076$ ppm reveals a substantially lower s electron density at the tin nuclear site as

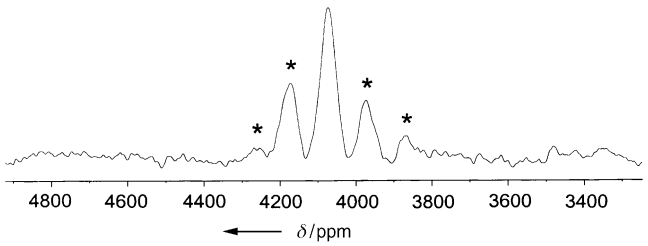

Figure 3. ^{119}Sn MAS NMR spectrum in Li_2AuSn_2 (spinning speed 14 kHz). The MAS spinning side bands are marked by asterisks.

compared to that in LiAuSn ($\delta = 5183$ ppm). The well-defined spinning side bands reveal a chemical shift anisotropy around 500 pm consistent with the noncubic symmetry evident from the crystal structure. The MAS linewidth of 7.2 KHz is considerable, suggesting a distribution of isotropic Knight shifts, which is indicative of some disorder in the static and/or electronic structure. Considerably wider ^{119}Sn Knight shift distributions, however, have been observed in $LiAg_2Sn$,[13] $LiRhSn_4$, and $LiIrSn_4$.[10]

The ^{119}Sn Mössbauer spectrum of Li_2AuSn_2 (Figure 4) shows a signal at an isomer shift of $\delta = 2.15(2)$ mm s^{-1} and a

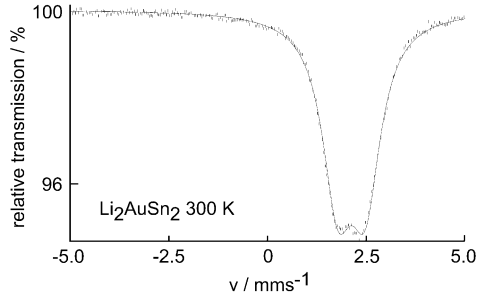

Figure 4. ^{119}Sn Mössbauer spectrum of Li_2AuSn_2 at room temperature.

linewidth of $\Gamma = 0.96(4)$ mm s^{-1}. The non-cubic local environment of the tin atoms is reflected by a quadrupolar splitting of $\Delta E_Q = 0.76(3)$ mm s^{-1}. All of these parameters are typical for those measured in transition-metal stannides.[13]

Figure 5 shows the ^7Li MAS NMR spectrum at room temperature. The observed single central peak confirms the existence of a unique lithium site as found from single-crystal

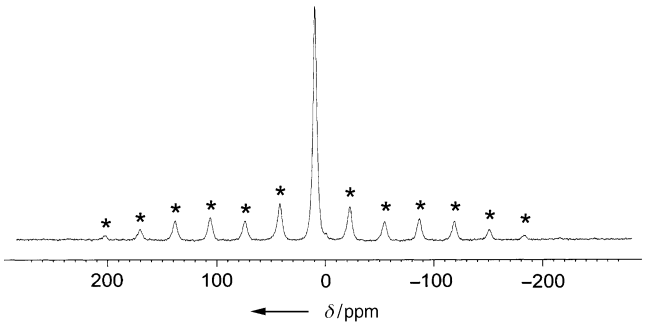

Figure 5. Experimental ^7Li MAS-NMR spectrum of Li_2AuSn_2 at room temperature. Spinning side bands are marked by asterisks.

X-ray diffraction data. The isotropic shift of 9.7 ppm indicates a rather small Knight shift contribution, consistent with a high degree of ionicity in the lithium bonding state. This behavior differs from the situation in binary lithium tin alloys ($Li_{2.2}Sn$, $Li_{4.4}Sn$), where NMR measurements reveal substantially larger Knight shifts.[26,27] The central ^7Li MAS-NMR peak of Li_2AuSn_2 is flanked by a spinning sideband manifold, arising from the $|1/2> <-> |3/2>$ satellite transitions broadened by first-order quadrupolar perturbations. Simulation of this side band manifold yields a nuclear electric quadrupolar coupling constant $C_Q = 52$ kHz and an asymmetry parameter $\eta = 0.9$ at room temperature. The small value of C_Q is consistent with the relatively high lithium site symmetry found from the crystal structure. Figure 6

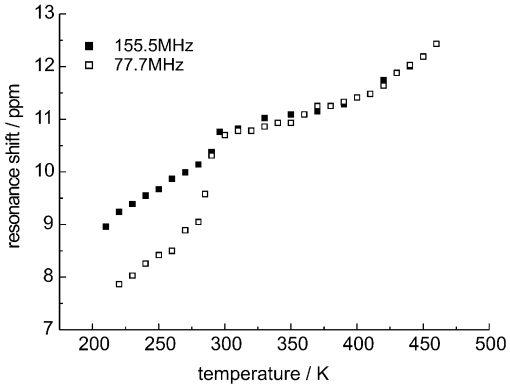

Figure 6. Temperature-dependent resonance shift of ^7Li MAS-NMR spectra in Li_2AuSn_2.

indicates that the ^7Li resonance shift is somewhat temperature-dependent, indicating a slight increase in Knight shift at higher temperatures. We also note the somewhat unusual observation that below 290 K the resonance shift depends

on the resonance frequency (155.5 versus 77.7 MHz), which, in turn, is governed by the magnetic field strength B_o. The specific field dependence observed (lower values of B_o producing lower values of the resonance shift) indicates that this effect is produced from a second-order quadrupolar perturbation. It is well known that such perturbations produce an upfield contribution to the resonance shift proportional to the inverse of the magnetic field strength.[28] As Figure 6 indicates, the effect is operative at low temperatures and disappears above 290 K. This finding suggests that the ^{7}Li nuclear electric quadrupolar interaction (and hence the second-order quadrupolar shifts) are averaged out at higher temperatures, suggesting the activation of a dynamic process involving the lithium atoms. More evidence for lithium dynamics is presented in the section below.

Evidence for lithium mobility: Figure 7 reveals that in the temperature range 240 K $< T <$ 390 K, the spinning side band manifold associated with the quadrupolar satellite transitions suffers serious broadening effects, indicating that the nuclear electric quadrupolar couplings are being increasingly averaged out by the lithium ionic motion. In the region of spinning side band coalescence, the condition $\omega_q\tau_c \sim 1$ is fulfilled, where τ_c is the motional correlation time and $\omega_q = \pi C_q$ (for spin 3/2 nuclei) is the quadrupolar frequency. The lithium motional process can be characterized in more quantitative terms on the basis of a temperature-dependent analysis of the ^{7}Li static spectra. Figure 8 and 9 show such data measured at 155.5 MHz over the temperature range 180 K to 440 K and at 77.7 MHz from 490 K to 810 K, respectively. The temperature-dependent half height line widths are plotted in Figure 10. The results obtained at both field strengths are identical within experimental error, suggesting that the chemical shift or Knight shift anisotropy and second-order quadrupolar coupling effects make only minor contributions to the lineshape. We can thus conclude that the static linewidth is governed by magnetic dipole–dipole interactions.

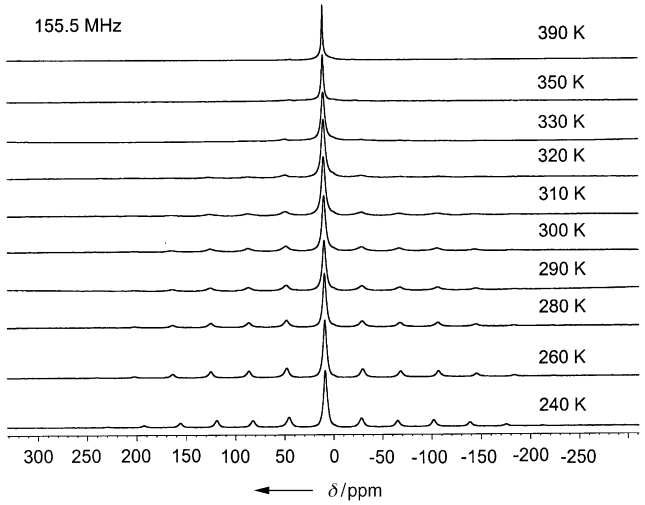

Figure 7. ^{7}Li MAS-NMR spectra in Li_2AuSn_2 within the temperature range from 240 K to 390 K at 155.5 MHz.

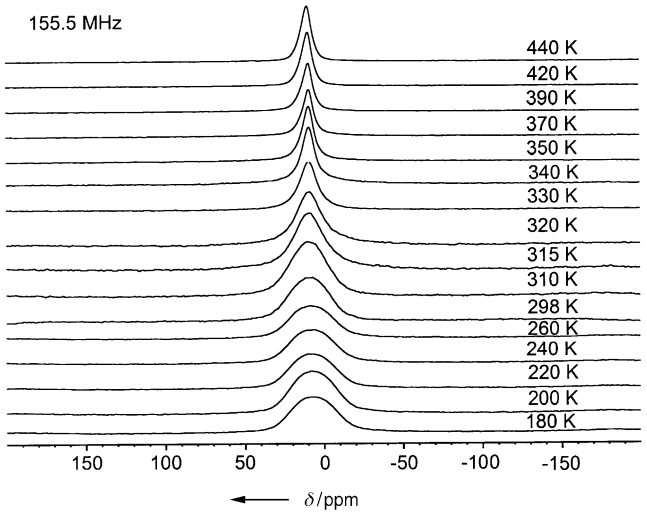

Figure 8. Static ^{7}Li NMR spectra in Li_2AuSn_2 within the temperature range from 180 K to 440 K at 155.5 MHz.

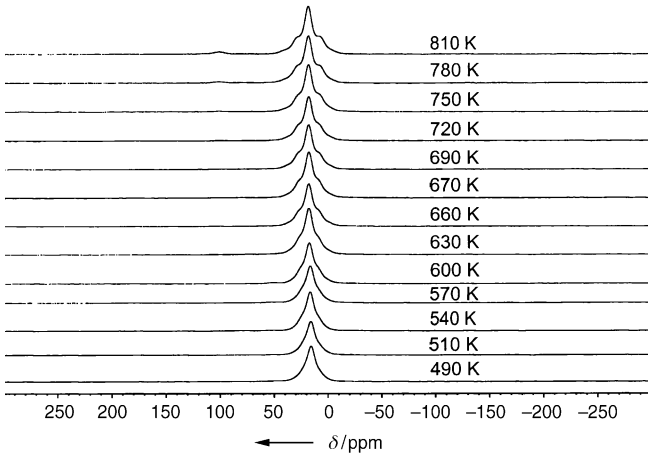

Figure 9. Variable-temperature ^{7}Li NMR spectra of Li_2AuSn_2 at 77.7 MHz within the temperature range from 490 K to 810 K.

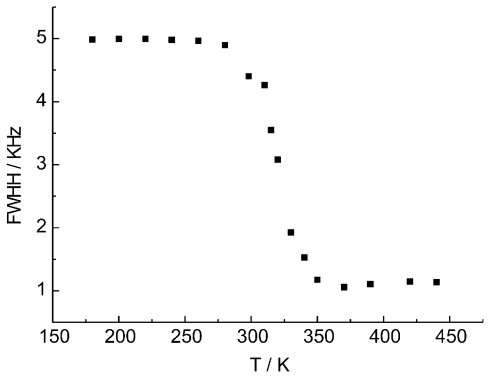

Figure 10. Temperature-dependent static ^{7}Li NMR line width at 155.5 MHz in Li_2AuSn_2 within the temperature range 180 K–440 K.

Among these, the homonuclear ^{7}Li–^{7}Li interactions are by far the dominant ones, owing to the large natural abundance of the ^{7}Li isotope and its high gyromagnetic ratio. The heteronuclear dipole–dipole interactions are negligible since the

natural abundances of ^{117,119}Sn are only near 8%. Application of the van Vleck formula[29,30] using the known internuclear distances from the crystal structure yields a contribution of M_2 (^{7}Li–^{7}Li) = 147.1 kHz^2. Approximating the lineshape by a Gaussian, this M_2 value implies a rigid lattice full width at half height of $\Delta = (8\ln 2 \cdot M_2)^{1/2}/2\pi = 4.55$ kHz. The experimental value measured (4.9 kHz) is slightly higher, possibly reflecting deviations from a Gaussian shape and minor linewidth contributions from other sources.

At sufficiently low temperatures ($T < 260$ K) the linewidths are essentially constant indicating that on the kHz time scale the lithium atoms remain at their own fixed positions in the rigid structure. Above 300 K, however, a mixed Gauss/Lorentz curve gives the best fit to experimental lineshapes, and the linewidths decrease sharply to an essentially constant plateau value of 0.9 KHz at and above 350 K. This effect reflects the dynamic averaging of the ^{7}Li dipolar interactions by lithium ion diffusion. The residual linewidth measured at high temperatures is most likely governed by transverse relaxation caused by fluctuating nuclear electric quadrupolar interactions. The corresponding activation energy of lithium ion diffusion in Li_2AuSn_2 is 27.4 kJ mol^{-1} as calculated from the equation $\Delta = A\exp(E_a/RT)$, where Δ is the full width at half height and A is constant (see Figure 11). This value is comparable in magnitude to the

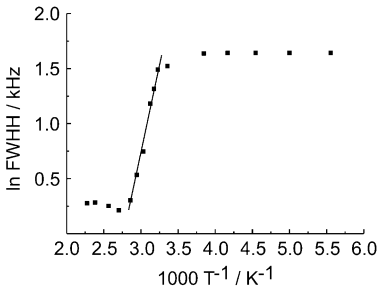

Figure 11. Arrhenius plot of ^{7}Li NMR static linewidth in the transition region, resulting in the activation energy given in the text.

value of 33.3 kJ mol^{-1} in $LiAg_2Sn$[13] and significantly smaller than the value of 46.0 kJ mol^{-1} previously measured in the Zintl phase LiCd, where motional narrowing was observed above 453 K.[31]

More detail about the lithium motional process is revealed by the observation of residual static quadrupolar splittings which are still apparent at high temperatures. The presentations of the static spectra in Figure 8 and 9 emphasize the central $|1/2><->|-1/2>$ transitions, whereas the $|1/2><->$ $|3/2>$ and $|-1/2><->|-3/2>$ coherences, which give rise to the spinning side band pattern in Figure 7 are too broad to be visible over this selected spectral range. Above 500 K, however, the magnitude of the nuclear electric quadrupolar coupling constant is significantly reduced by fast lithium motion. As a result, the central resonances are now symmetrically flanked by satellite shoulders. From the splittings one can estimate a residual nuclear electric quadrupolar coupling constant around 2.0 kHz. The presence of this residual splitting indicates that the lithium atomic motion is not completely isotropic even in this temperature region. Rather the exchange must occur among a limited number of sites only, preserving a small degree of anisotropy in the static spectra in the fast motion limit.

Independent information about lithium dynamics on the MHz time scale is provided by ^{7}Li spin-lattice relaxation studies. At all the investigated temperatures, the return of the nuclear magnetization to equilibrium is found to be exponential and unique T_1 values could be extracted from each experiment. Figure 12 shows the ^{7}Li spin-lattice relaxa-

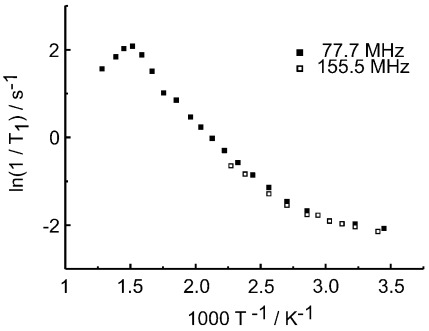

Figure 12. ^{7}Li spin-lattice relaxation time as a function of reciprocal temperature in Li_2AuSn_2.

tion rate as a function of reciprocal temperature. A maximum near 660 K clearly reveals the occurrence of lithium dynamics where $\omega_o\tau_c \sim 1$. Assuming the applicability of the Bloembergen–Purcell–Pound (BPP) theory,[32] an activation energy of 28.6 ± 0.8 kJ mol^{-1} was determined from the slope of $\ln(1/T_1)$ versus $1/T$ (between 490 K and 600 K). This value is in excellent agreement with the value of 27.4 ± 1.3 kJ mol^{-1} calculated from the motional narrowing effect in the static spectra at $310\ \mathrm{K} < T < 350$ K. The apparent validity of the BPP theory in the description of lithium dynamics in Li_2AuSn_2 is consistent with a sufficiently random lithium motion described by a single exponential correlation function.

For $T < 440$ K, the relaxation appears to be dominated by a frequency-independent electronic contribution arising from unpaired spin density in the conduction band. In this temperature range, the relaxation behavior of Li_2AuSn_2 corresponds closely to that observed in numerous other lithium stannide materials.[10,13] On the other hand, the observation of a distinct relaxation contribution that is attributable to lithium motion is unique for Li_2AuSn_2 and has not been observed in any other lithium stannide material so far.

Conclusion

In summary, all of the NMR results presented here indicate that Li_2AuSn_2 is characterized by an exceptional degree of lithium ionic mobility which sets this compound apart from all of the other binary and ternary lithium stannides investigated so far. Since the lithium site located in extended channels formed by a three-dimensional [$AuSn_2$] polyanion is not fully occupied, the high mobility of lithium may be under-

stood by the existence of accessible vacancies. The detailed mechanism of ionic motion and the optimization of this system for potential battery electrode applications will be the subject of future investigations.

Acknowledgement

We thank H.-J. Göcke for the work on the scanning electron microscope, Dr. W. Buscher and Dipl.-Chem. A. Klostermeyer for the ICP analyses, and the Degussa-Hüls AG for a generous gift of gold wire. Financial support by the Deutsche Forschungsgemeinschaft through SFB 458 "Ionenbewegung in Materialien mit ungeordneten Strukturen" and by the Fonds der Chemischen Industrie is gratefully acknowledged.

[1] J. Yang, M. Winter, J. O. Besenhard, *Solid State Ionics* **1996**, *90*, 281.
[2] S. Machill, D. Rahner, *J. Power Sources* **1995**, *54*, 428.
[3] J. O. Besenhard, J. Yang, M. Winter, *J. Power Sources* **1997**, *68*, 87.
[4] T. Koyamada, H. Ishihara, *Electrochim. Acta* **1995**, *40*, 2173.
[5] M. M. Thackeray, K. D. Kepler, J. T. Vaughey, Patent No. WO 2000003443, Application No. WO 1999-US12868.
[6] Y. Nitta, H. Shimamura, K. Okamura. (Matsushita Electric Industrial Co., Ltd., Japan). Jpn. Kokai Tokkyo Koho (**1999**), Application: JP 97–196705 19970723.
[7] A. Saito, Y. Aono, T. Horiba, H. Kodama, T. Dozono, M. Inagaki. (Hitachi, Ltd., Japan). Fr. Demande (**1996**), Application: FR 96–7281 19960612.
[8] R. Pöttgen, Zh. Wu, R.-D. Hoffmann, G. Kotzyba, H. Trill, J. Senker, D. Johrendt, B. D. Mosel, H. Eckert, *Heteroat. Chem.* **2002**, *13*, 506.
[9] Zh. Wu, R.-D. Hoffmann, R. Pöttgen, *Z. Anorg. Allg. Chem.* **2002**, *628*, 1484.
[10] Zh. Wu, H. Eckert, J. Senker, D. Johrendt, G. Kotzyba, B. D. Mosel, H. Trill, R.-D. Hoffmann, R. Pöttgen, *J. Phys. Chem. B* **2003**, *107*, 1943.
[11] R.-D. Hoffmann, D. Johrendt, Zh. Wu, R. Pöttgen, *J. Mater. Chem.* **2002**, *12*, 676.
[12] Zh. Wu, H. Eckert, B. D. Mosel, R. Pöttgen, *Z. Naturforsch. Teil. B* **2003**, *58*, 501.
[13] Zh. Wu, R.-D. Hoffmann, D. Johrendt, B. D. Mosel, H. Eckert, R. Pöttgen, *J. Mater. Chem.* **2003**, *13*, 2561, and references therein.
[14] Zh. Wu, H. Eckert, B. D. Mosel, R. Pöttgen, R.-D. Hoffmann, D. Johrendt, *Z. Kristallogr.* **2003**, *20*, 159.
[15] R. Pöttgen, T. Gulden, A. Simon, *GIT Labor-Fachz.* **1999**, *43*, 133.
[16] K. Yvon, W. Jeitschko, E. Parthé, *J. Appl. Crystallogr.* **1977**, *10*, 73.
[17] G. M. Sheldrick, SHELXS-97, Program for the Solution of Crystal Structures, University of Göttingen, Germany, 1997.
[18] G. M. Sheldrick, SHELXL-97, Program for Crystal Structure Refinement, University of Göttingen, Germany, 1997.
[19] J. Emsley, *The Elements*, Oxford University Press, 3rd edn, **1999**.
[20] R. Pöttgen, U. Häussermann, R.-D. Hoffmann, Zh. Wu, unpublished results.
[21] J. Donohue, *The Structures of the Elements*, Wiley, New York, **1974**.
[22] G. Kienast, J. Verma, *Z. Anorg. Allg. Chem.* **1961**, *310*, 143.
[23] E. A. Axtell, J.-H. Liao, M. G. Kanatzidis, *Inorg. Chem.* **1998**, *37*, 5583.
[24] F. Q. Huang, Y. Yang, C. Flaschenriem, J. A. Ibers, *Inorg. Chem.* **2001**, *40*, 1397.
[25] C. Lupu, J.-G. Mao, J. W. Rabalais, A. M. Guloy, J. W. Richardson, Jr., *Inorg. Chem.* **2003**, *42*, 3765.
[26] G. R. Goward, L. F. Nazar, W. P. Power, *J. Mater. Chem.* **2000**, *10*, 1241.
[27] Y. Wang, J. Sakamoto, C. K. Huang, S. Surampudi, S. G. Greenbaum, *Solid State Ionics* **1998**, *110*, 167.
[28] A. G. Marshall, T. C. L. Wang, C. E. Cottrell, L. G. Werbelow, *J. Am. Chem. Soc.* **1982**, *104*, 7665.
[29] J. H. van Vleck, *Phys. Rev.* **1948**, *54*, 682.
[30] A. Abragam, *Principles of Nuclear Magnetism*, Clarendon Press Oxford, **1961**.
[31] C. van der Marel, W. van der Lugt, *J. Phys. F* **1980**, *10*, 1177.
[32] N. Bloembergen, E. M. Purcell, R. V. Pound, *Phys. Rev.* **1948**, *73*, 679.

Received: August 25, 2003 [F5479]